A Parametric Study of the Effect of Roof Height and Morphology on Air Pollution Dispersion in Street Canyons

H. Wen[1] and L. Malki-Epshtein[*]

Department of Civil, Environmental and Geomatic Engineering, University College London (UCL), Gower street, London WC1E 6BT, United Kingdom

*Corresponding author. Department of Civil, Environmental and Geomatic Engineering, University College London (UCL), Gower Street, London WC1E 6BT, United Kingdom

Email address: l.malki-epshtein@ucl.ac.uk

[1]Present address: Wind Power Research and Development Centre, Zhejiang University, 5-102 Jianhua Park, Hangzhou China

KEYWORDS: CFD, Air Quality, Street Canyons, Urban pollution, Airflow

HIGHLIGHTS

- Parametric study of airflow and pollution in street canyons of different morphologies
- Conventional pitched roofs increase pollution concentration for most morphologies
- Pollution and airflow sensitive to roof slope and roof arrangement morphology
- Morphology of upstream streets affects pollution concentration downstream
- Interaction between parameters complex; results are variable and case specific

ABSTRACT

We investigate the effect of conventional pitched roofs on ventilation and pollution in street canyons using Computational Fluid Dynamics and a parametric approach. We studied parallel street canyons with several street morphologies, created by assigning a set of streets with pitched roofs, and varying their pitch and arrangement for three different height-to-width aspect ratios. The distribution of flow properties and pollution concentrations within the street canyons are examined and the effect of different parameter combinations is assessed. We find the relationship between these properties and the street morphology to be complex and case specific.

For most morphologies, the pitched roofs lead to higher average pollution concentrations, and in some cases to pollution hotspots near emission sources especially on the leeward side. The pitched roofs are rarely beneficial to ventilation of the street canyons, but a few roof arrangements lead to reduced concentrations on the windward side. Roof slope is shown to significantly relate to both average pollution concentrations and their distribution inside the street; in some street geometries more than others. The results have implications for pedestrian and residential pollution exposure, and for conservation of building facades on historical buildings.

1 Introduction

Street canyons, where long narrow streets are bordered by a continuous row of buildings on both sides, are a typical urban geometry in many European cities. These streets are known to suffer from poor ventilation, especially when the buildings are tall and the streets are narrow, leading to accumulation of pollution and heat in the streets. As air quality in urban environments deteriorates and the consequences of this on the health of pedestrians, drivers and residents are apparent, there is a growing recognition that we need to understand the impact of street and building geometries on air quality.

The fundamental flow regimes and pollutant dispersion principles in street canyons are generally well-understood. The pioneering study of Oke (1988), identified that when the background wind is perpendicular to the street, this results in three fundamental flow regimes between buildings depending on the aspect ratio of the building height to the street width: H/W. When the street is narrow (H/W>0.7), the resulting flow regime is skimming flow, which is characterized by recirculating airflow within the street and is adverse for ventilation. Meroney et al. (1996) studied pollutant dispersion from line sources and highlighted the difference in dispersion regimes in open country and in urban settings. Sini et al. (1996) modelled thermal effects on airflow and pollutant dispersion in street canyons, and Kastner-Klein and Plate (1999) tested the significance of several street geometries in affecting street canyon flow. At a more detailed level, the dispersion around buildings is governed by a complex interaction between the atmospheric flow and the flow around buildings (Tominaga and Stathopoulos, 2013).

Many previous experimental and numerical studies are based on idealized building and street morphologies, which are rarely seen in the real world. In particular, there have been many studies assuming flat-roof buildings throughout the length of the street, for example, Uehara et al. (2000), Gu et al. (2011), Wen et al. (2013), Guillas et al. (2014) and Gromke and Blocken (2015). Karra et al (2017) model a series of consecutive street canyons in a water channel in the laboratory and visualise with PLIF and PIV both the velocities and the release of dye from the center of the street.

Roofs are usually designed to have slopes to avoid accumulation of rain water and snow. The detailed construction of a roof is determined by locally available materials, structural factors, usage of the roof space, walkability, aesthetic architectural factors and local custom. These factors will then determine the shape of the roof and its pitch. The slope of a pitched roof is usually defined by the run divided by the rise, as illustrated in Figure 1.1 below. It is conventionally expressed as a ratio with 12 in the denominator. According to the ratio, pitched roofs can be classified into non-perfect flat roof (ratio less than 2:12), low-slope roof (2:12 to 4:12), conventional roof (4:12 to 9:12) and steep-slope roof (>9:12) (Schmid, 2014). Pitched roofs on large buildings usually have low rises, considering the cost of materials, labour and space usage (Reid, 2000). Conventional roofs are more commonly seen on residential buildings rather than large commercial or public buildings; steep-slope roof is a typical design in northern regions to prevent accumulation of snow (Reid, 2000).

Roof structure has been found to have a significant aerodynamic impact on airflow and pollutant dispersion around a building in a number of studies. Since pitched roofs are commonly found in European cities, they have been more regularly studied than other roof types. Rafailidis (1997) carried out an experimental study to compare flat roofs with 12:12 pitched roofs. From his measurements, he concluded that: "*street canyon re-aeration is influenced mainly by vertical dispersion of the pollutants (enhanced by vertical turbulence) and their subsequent advective removal horizontally by the oncoming wind".* He found that although the pitched roofs led to weaker horizontal advection at roof height than flat roofs, they significantly increased turbulence intensity above roof height (H) and up to the height of 3H. Thus, Rafailidis (1997) claimed that pitched roofs can be an effective means to increase wind-driven natural ventilation at the street opening. Leitl and Meroney (1997), Theodoridis and Moussiopoulos (2000), and Xie et al. (2005) used CFD models to reproduce Rafailidis' experiment and validated their models based on the concentrations measured by Rafailidis. All of them calculated pollution concentrations on the building walls, finding them to be higher on the windward side than on the leeward side. This result was contradictory to the typical pollutant distribution found in street canyons. However, the use of CFD modelling allowed full exploration of the flow patterns, and revealed that in this particular scenario, where the effective aspect ratio of the street was high, two counter-rotating vortices were formed below the roof-top level, which therefore led to these unexpected results.

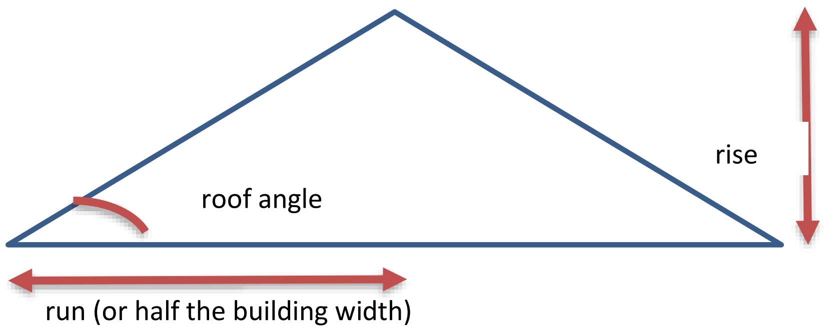

Figure 1.1: A typical pitched roof.

Louka et al. (1998) conducted field measurements between two long farm buildings with 9.6:12 pitched roofs. They found that the pitched roofs greatly affected eddy size distribution in the street canyon as well as air exchange between the street and the atmosphere. In addition, their measurements suggested that the typical single vortex flow pattern did not exist in their case. Kastner-Klein et al. (2004) carried out a few experimental studies of flat roofs and 8:12 pitched roofs in urban street canyons. They found that the presence of this pitched roof on the leeward building generated unique flow patterns on the mid-vertical plane of the street: no vortex was formed on the mid-vertical plane; instead, air flowed from the windward side to the leeward side and from the bottom upwards. This observation indicated that the flow structure in the street was three-dimensional and there existed strong air flow along the length of the street.

There are a limited number of studies in the literature of street canyons with various roof shapes. Llaguno-Munitxa et al. (2017) studied different roof shapes such as pitched, dome and terraced roofs and demonstrated the flow patterns around the buildings with these roofs. Yassin (2011) tested several roofs with different shapes and slopes and found that both factors had an important effect on flow field and pollutant distribution. Takano and Moonen (2013) focused their efforts on the roof slope of slanted roofs (pitched only on one side). They found that increasing the roof slope resulted in the transition from single-vortex flow regime in the street canyon to a double-vortex flow regime and found that the critical angle for the transition was around 18 degrees for a downward slanted roof. Most previous studies demonstrated the importance of roof slope due to its aerodynamic effects on airflow, however only a limited set of roof slopes have been studied before. These were limited mainly to steep slopes with rise-to-run ratios ranging from 8:12 to 12:12, which are less common in street canyons in real urban settings. Huang et al. (2009) analysed urban morphological arrangements of slanted roofs and pointed out that a slanted roof on the leeward building had much stronger aerodynamic impacts than the same roof geometry on the windward building.

Thus, both roof geometry and the arrangement of the roofs on both sides of the street canyon play a key role in affecting the airflow, but most previous work has only focused on either the geometry or the morphology. The interaction between them is not yet clear, and in particular it is unclear how the airflows are affected by these factors, for a wide range of street aspect ratios.

In this study we conduct a parametric study of urban street canyons with pitched roofs using Computational Fluid Dynamics (CFD). The study considers a set of realistic roof slopes, positions those is several arrangements to create different street morphologies and attempts this for three different street canyon aspect ratios. The paper is structured as follows. Section 2 introduces the numerical modelling methods and settings, and describes the selected street canyon configurations for a total of thirty-nine cases, which are generated by systematically varying three geometric parameters. Section 3 describes the modelled results inside the streets, focusing on flow patterns, flow properties and the distribution of pollution concentration; the results for different cases are analysed to examine the impacts of the three parameters. Section 4 summarises the main findings. The paper concludes by discussing under which conditions, pitched roofs are beneficial or detrimental for street ventilation and pollutant removal and discusses their significance for urban planning.

2 Numerical model

The CFD modelling was carried out in ANSYS FLUENT 12.0. To reduce computational cost, all the CFD models were based on steady-state assumption and full-scale two-dimensional geometry. The background wind was set to be perpendicular to the streets, and the pollutant concentration in the background wind was set to zero. The typical street canyon flow case used for validation of the model is presented in Section 2.1. The full details of the numerical methods and CFD settings are introduced in Sections 2.2 and 2.3. Section 2.4 gives a full description of the CFD models employed in this parametric study.

2.1 Validation

Validation was carried out by modelling the wind tunnel experiments of Kastner-Klein and Plate (1999), which correspond to three consecutive ideal homogeneous street canyon configurations with flat roofs on the adjacent buildings. The CFD model was performed at the wind tunnel scale. For full details of the validation procedure, see Wen (2017). Validation data sets are rare for the parameter space we explored. This set of experiments was useful as it was a set of experiments that had both velocity and concentration measurements. It was important that the buildings modelled were also sufficiently long to produce approximately two dimensional flow that could be reasonably modelled in 2D CFD. Their data set was appropriate for our cause yet was only carried out for the flat roof case. Hence we used this as our validation case and our reference case in the parametric study was selected as the flat roof case.

The full technical details of the wind-tunnel experiment can be found in Kastner-Klein (1999). The main experimental setup is introduced here and presented schematically in Figure 2.1 below. Four parallel buildings were placed in the wind tunnel, creating three street canyons with an aspect ratio of one. The background wind was perpendicular to the street axes. All the buildings had a 12cm×12cm square-shape cross-section and were as long as 180cm in the span-wise direction; the length of the buildings (L=15H) was found to be sufficiently long to produce two-dimensional flow and dispersion characteristics in the centre of the street . Tracer gas was released from a line source located at the bottom of the last street canyon. The line source was placed either 3.5cm away from the leeward building or 3.5cm away from the windward building, which created two emission cases (Case 1 and Case 2 respectively). Concentration was measured on two side profiles at positions that were 0.7cm (or 0.05H) away from the building walls.

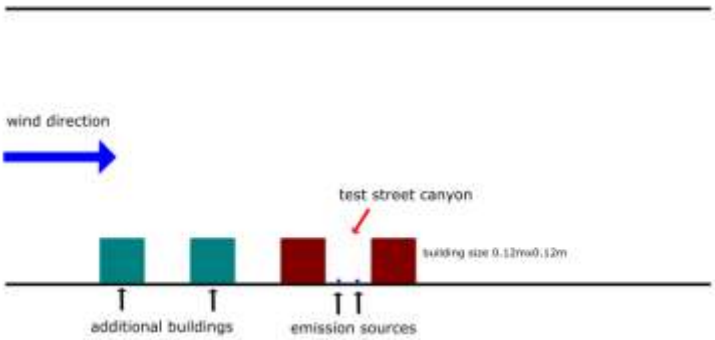

Figure 2.1: A sketch of Kastner-Klein and Plate's experimental setup. Replotted following Kastner-Klein (1999).

Flow patterns and properties in the CFD model were first compared with those in the experiments reported in Kastner-Klein (1999) to ensure the model achieves the correct flow. Following this, the pollutant concentrations were compared between the measurements and the modelling results for the two vertical profiles within the street canyon. Figure 2.2 below presents the pollutant concentrations on the vertical profiles (i.e., leeward side line and windward side line), where experimental measurements had been taken. The results are presented in a normalized form, to be comparable to the experimental data. There is a good agreement between the model results and the measurements, as seen in Figure 2.2: the predicted concentration profiles are very close to the experimental curves and in both cases match the measurements to within 5% on the leeward side, where the concentrations are greater, and to within 25% on the windward side where the concentrations are smaller.

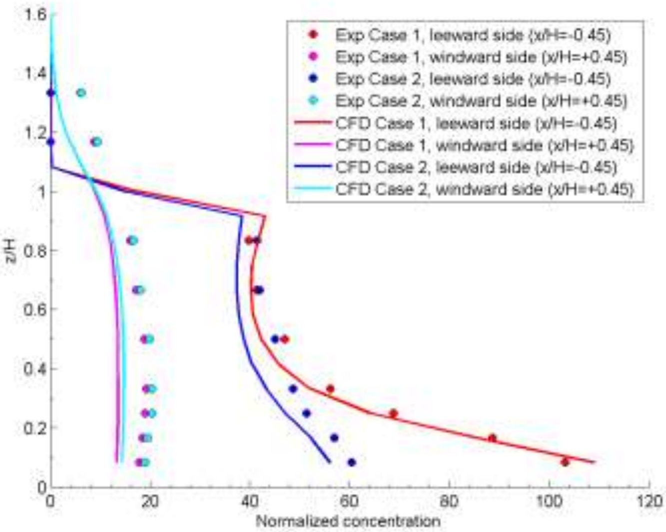

Figure 2.2: Normalised pollutant concentration on the leeward and windward side lines which are 0.7cm (or 0.05H) away from the building walls. Circle: experimental measurements from Kastner-Klein (1999), solid line: CFD results.

2.2 Numerical methods

The incompressible Reynolds-averaged Navier–Stokes (RANS) equations were solved across the computational domain. As we modelled cases with relatively low pitched roofs throughout our study, we tested two models in our validation that were known to predict well the flow on flat roofs in 2D and were the most widely used in the literature; these were the standard k-ε model and the RNG k-ε model. The standard k-ε model was selected for turbulence closure, as it was found in our validation simulations to perform best for those street canyon cases.

The governing equations are given below; the scalable wall function was used to model near-wall flow. They were found to be relatively economic and reliable options to model street canyon flow according to our previous experience. For full details about the model, see Wen (2017).

$$\frac{\partial u_i}{\partial x_i} = 0$$

$$\frac{\partial u_i}{\partial \mathrm{t}} + \frac{\partial (u_i u_j)}{\partial x_j} = -\frac{1}{\rho}\frac{\partial \mathrm{p}}{\partial x_i} + \frac{\partial}{\partial x_j}\left[\nu \frac{\partial u_i}{\partial x_j}\right] - \frac{\partial}{\partial x_j}\left(\overline{u_i{}' \ u_j{}'}\right)$$

$$\frac{\partial k}{\partial t} + \frac{\partial (k u_i)}{\partial x_i} = \frac{\partial}{\partial x_i}\left[\left(\nu + \frac{\nu_t}{\sigma_k}\right)\frac{\partial k}{\partial x_i}\right] + \overline{u_i{}' \ u_j{}'}\,\frac{\partial u_j}{\partial x_i} - \varepsilon$$

$$\frac{\partial \varepsilon}{\partial t} + \frac{\partial (\varepsilon u_i)}{\partial x_i} = \frac{\partial}{\partial x_j}\left[\left(\nu + \frac{\nu_t}{\sigma_\varepsilon}\right)\frac{\partial \varepsilon}{\partial x_i}\right] + C_{1\varepsilon}\frac{\varepsilon}{k}\overline{u_i{}' \ u_j{}'}\,\frac{\partial u_j}{\partial x_i} - C_{2\varepsilon}\frac{\varepsilon^2}{k}$$

$$-\overline{u_i{}' \ u_j{}'} = -\frac{2}{3}k\delta_{ij} + \nu_t\left(\frac{\partial u_i}{\partial x_j} + \frac{\partial u_j}{\partial x_i}\right)$$

$$\nu_t = C_\mu \frac{k^2}{\varepsilon}$$

where x_i is the *i*th Cartesian coordinate, u_i and u_i' are the *i*th mean and fluctuating velocities respectively, the overbar stands for time average, ρ is the density of air, p in the mean pressure, ν and ν_t are the kinematic viscosity and kinematic eddy viscosity respectively, k is the turbulent kinetic energy, ε is the turbulent dissipation and δ_{ij} the Kronecker delta. C_μ=0.09, $C_{1\varepsilon}$=1.44, $C_{2\varepsilon}$=1.92, σ_k=1.0 and σ_ε=1.3 are the model constants.

A convection-diffusion equation for passive scalar is used to model emitted pollutants through the application of User-Defined Scalar in FLUENT (ANSYS Inc., 2009).

$$\frac{\partial c}{\partial t} + \frac{\partial (c u_i)}{\partial x_i} = \frac{\partial}{\partial x_j}\left(\left(\Gamma + \frac{\nu_t}{Sc_t}\right)\frac{\partial \mathrm{c}}{\partial x_j}\right)$$

where c is the pollutant concentration, Γ is the molecular diffusion coefficient and Sc_t is the turbulent Schmidt number. A range of Schmidt numbers were tested for street canyons, in the range of 0.7 to 0.9 on the basis of previous work on street canyons. We applied a constant value of 0.9, which gave the best prediction of pollutant dispersion in two-dimensional street canyons, in agreement with the experimental dataset used for validation.

It is vital to accurately simulate the atmospheric boundary flow in the computational domain to obtain reliable predictions of the pollution dispersion processes in the streets (Tominaga and Stathopoulos, 2013). The same boundary conditions are applied for all simulations, and these are summarized in Table 2-1 below. The boundary types and the size of computational domain follow "Best Practice Guideline for the CFD Simulation of Flows in the Urban Environment" (Franke et al., 2007). The inlet velocity profile is defined as the original wind profile given by Kastner-Klein (1999). The profiles of turbulent kinetic energy k and turbulent dissipation ε are specified according to "AIJ Guidelines for Practical Applications of CFD to Pedestrian Wind Environment around Buildings" (Tominaga et al., 2008). Each emission source is defined as a velocity inlet with extremely small velocity and zero turbulence intensity so that it will not affect the flow inside the street.

Inlet boundary	Velocity inlet (6H away from the first building, where H is the building height) $U = U_{ref}\left(\frac{z}{z_{ref}}\right)^{\alpha}$, where: U_{ref}=7.7m/s is the velocity at the reference height z_{ref}=72m, α=0.18 is the power-law index, and z is the height from the ground. The displacement height is ignored. $k = \left[0.1U\left(\frac{z}{z_{ref}}\right)^{-\alpha-0.05}\right]^2$ $\varepsilon = C_{\mu}^{1/2} k \frac{U_{ref}}{z_{ref}} \alpha \left(\frac{z}{z_{ref}}\right)^{\alpha-1}$ where C_{μ}=0.09 is one of the empirical constants of the standard k-ε model referred to earlier
Outlet boundary	Outflow (15H away from the last building)
Top Boundary	Symmetry (12H away from the ground)
Ground	Smooth wall
Building surfaces	Smooth wall
Emission sources	Velocity inlet with extremely small velocity and zero turbulence intensity; all the sources have the same emission rate

Table 2-1: A summary of the boundary conditions

2.3 CFD settings

In the CFD model, mesh sensitivity tests were carried out on the profiles corresponding to the experimental concentration profiles, and to the central vertical line corresponding to velocity measurements. The horizontal velocity *U*, vertical velocity *W*, turbulent kinetic energy *k*, and concentration *c* were solved under four different mesh resolutions to find the appropriate mesh resolution for all parameters. We used structured quadrilateral mesh, with inflation ratio of 1.2. For the validation model we found that mesh independence was achieved for velocity, TKE and concentrations with a fine mesh with 36 cells along the building height. However for the parametric study, considering the introduction of pitched roofs and the associated flow structure, 85 nodes were placed along the surface of the building in all simulations. This mesh is finer than the mesh resolutions used in many CFD simulations of street canyon flow, such as Solazzo et al. (2009), Koutsourakis et al. (2012) and Gromke and Blocken (2015). We found that this mesh resolution was fine enough to ensure mesh independent results. The total number of cells for each model was around 200,000.

The second-order upwind scheme was selected to discretize the momentum, turbulent kinetic energy, turbulent dissipation and passive scalar equations. Semi-Implicit Method for Pressure Linked Equations-Consistent (SIMPLEC) was used for pressure-velocity coupling. The RANS simulations were initialized with uniform velocity, TKE and dissipation along the stream-wise direction. The default under-relaxation factors were used for iterative calculations. Calculations were run until all the residuals dropped below 10-6. This residual threshold is sufficiently small to guarantee convergence (Franke et al., 2007).

2.4 Street canyon configurations

Each case simulates an idealized urban structure that consists of six equally spaced building rows, creating five consecutive homogeneous street canyons. We defined the third street canyon as the test canyon, and examined the flow and pollution in the fourth street canyon as well, in order to identify downstream effects. In the third and the fourth street canyons where flow is fully-developed, two emission sources were set on the ground of each street to model traffic emission. Each source was defined as 0.3m (equivalent to 0.025H) wide and 1m away from the leeward building or the windward building. This street configuration in the CFD simulation smooths turbulence, and leads to a well-developed urban boundary layer with stable flow in the third and fourth test streets. The impacts of the flow separation at the leading edge of the first building row and of the sixth building row, become negligible in the third and fourth streets. We found that for the reference case of flat roofs, , the CFD model for this configuration results in a stable vortex in the third street canyon, as we expect from extensive studies in the literature and as seen in the experiments of Kastner-Klein and Plate (1999) and in the physical models e.g. in Karra et al. (2017). The variations in street morphologies are achieved by varying three parameters in this study: the aspect ratio of the street (AR), the rise-to-run ratio of the pitched roofs, and the morphology of the roof arrangement.

All the buildings are 12m wide and 12m tall, whereas street width varies between 15m, 12m and 9m, resulting in three aspect ratios of building height to street width AR=0.8, AR=1.0 and AR=1.3, respectively.

The five street canyons have identical pitched roofs throughout, with different Cases defined by variation on the rise-to-run ratio of the pitched roofs. The pitched roofs in each case have the same pitch rise for all the streets. To generate different Cases the rise varies as R=1m, 2m and 3m, giving three rise-to-run ratios of: 2:12, 4:12 and 6:12.

The third street canyon, which is the test street, is flanked by various combinations of flat roofs and pitched roofs which create four different basic roof morphologies for the third street. The reference Cases A is that for which all roofs throughout are flat roofs. We thus have a total of 13 basic Case studies – repeated for each aspect ratio to a total of 39 unique Cases. It is worth noting that the fourth street is also of interest, and on this street there are three basic roof arrangements (since in that street the roof arrangements for cases B, C, and D are identical to cases H, I, and J respectively). However, these cases are preceded by *different* roof arrangements in the third street canyon. This determines the shape of the approach flow; thus these six cases are still unique with respect to the fourth street canyon properties.

The different street and roof geometries are each simulated separately, to a total of 39 simulations. Figure 2.3 below is a table that illustrates all the cases with AR=1.0, named as Cases 10A to 10M. The aspect ratio is indicated by the prefix number before the case index (i.e., 10 stands for AR=1.0, 13 for AR=1.3, 08 for AR=0.8); the case index A to M are used to represent the different morphologies described above. The pitch rise (R) of each case is also indicated in the figure. In the figure, each building colour represents a specific roof morphology for the third street canyon. These are:

- Black (reference case): flat roofs on all the buildings
- Red: flat roofs on the Leeward Building (LB) and on the Windward Building (WB)
- Green: flat roof on the LB and pitched roof on the WB
- Cyan: pitched roof on LB and flat roof on the WB
- Purple: pitched roof both on the LB and on the WB

For ease of reference, this colour scheme is maintained in subsequent figures throughout the article.

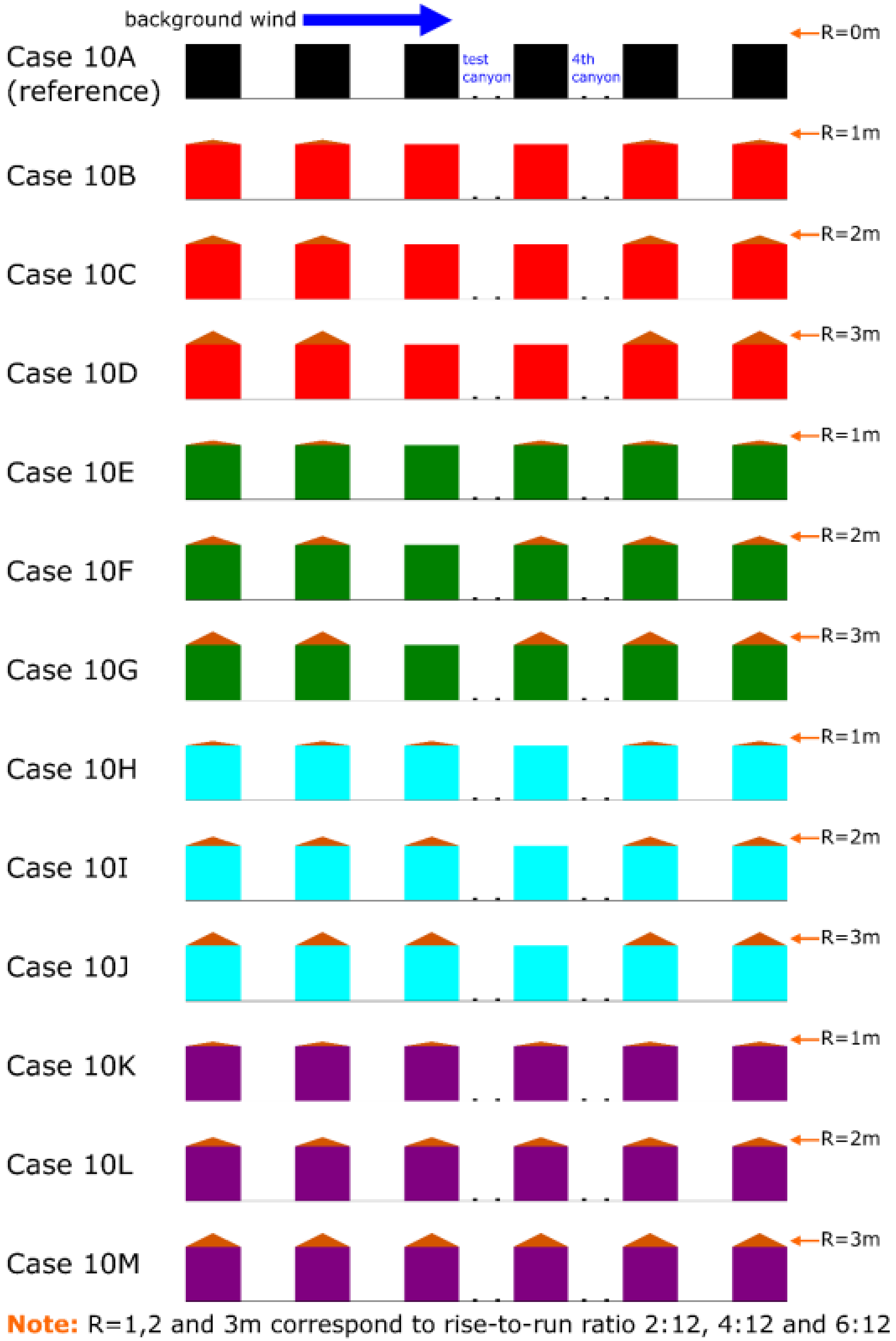

Figure 2.3: Sketches of the geometries for the cases with AR=1.0.

3 Results

Below is an analysis of the flow and concentrations in the street canyons in the model. The test street canyon is examined for flow patterns, flow properties, ventilation efficiency, pollution distribution patterns and detailed concentrations. For the fourth street canyon, adjacent to the test street, only pollution distribution and concentrations are analysed.

3.1 Flow patterns

The impacts of the three parameters on flow fields are examined first. For all examined cases, the streets with pitched roofs with a rise-to-run ratio of up to 6:12 exhibit a single vortex in each street canyon, similar to the reference case of street canyons with flat roofs on both sides. The flow patterns for four typical cases are shown in Figure 3.1 below, illuminating the most significant differences amongst all the cases. Two different street aspect ratios are examined: cases 10A and 10M correspond to AR=1.0 and cases 13A and 13M, to AR=1.3. Cases A are the reference cases of flat roofs, and cases M have pitched roofs on all streets.

We define the street as the area between the buildings up until the height of the base of the roof. It can be seen that a vortex flow pattern exists inside the third and fourth streets in all cases. The vortex shape mainly depends on the aspect ratio. Increasing the aspect ratio leads to the elongation of the vortex in the vertical direction, at least in the Aspect Ratio range studied here.

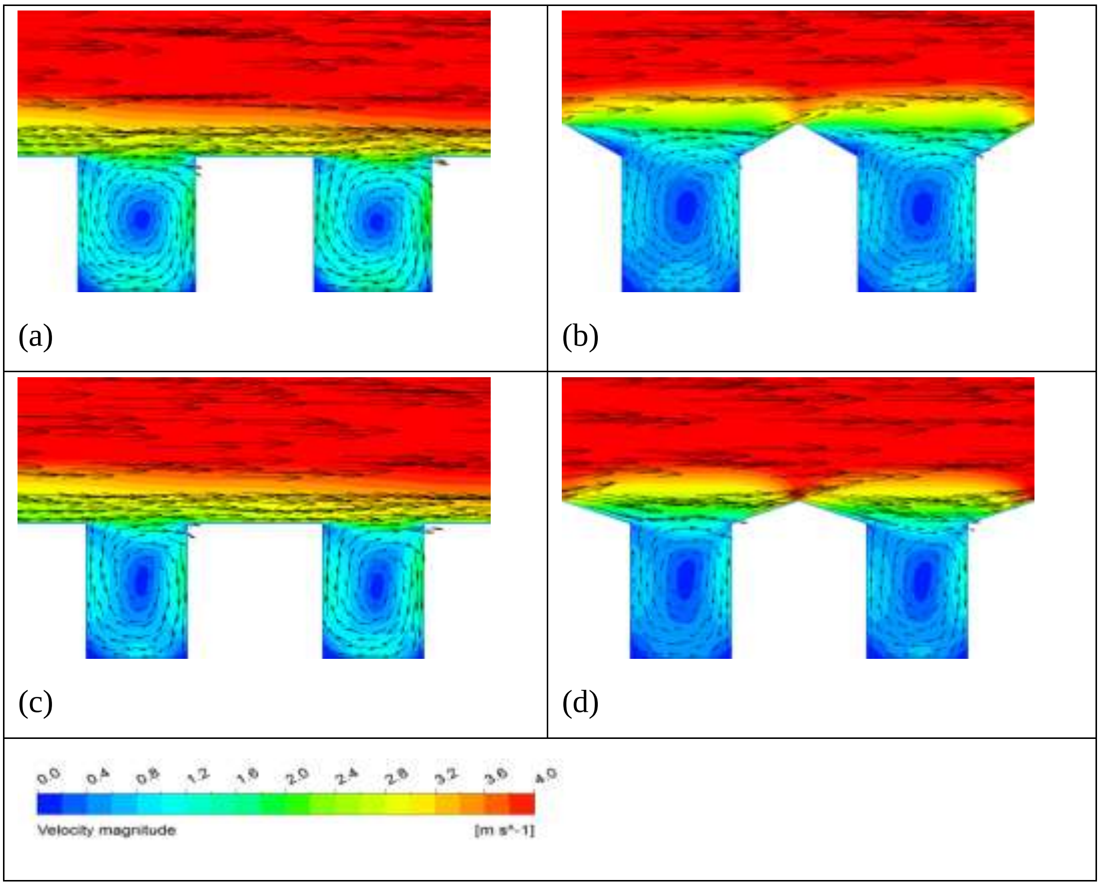

Figure 3.1: Combined velocity vector and velocity magnitude contour around the third and the fourth street canyons: (a) Case 10A, (b) Case 10M, (c) Case 13A, and (d) Case 13M.

The roof structure has a secondary effect on the vortex flow. As can be seen in Figure 3.1, high-rise pitched roofs disturb the flow above the street, leading to a thicker shear layer above the rooftops. Consequently, for the two cases with pitched roofs (i.e., Cases 10M and 13M in the figure), the vortex extends above the street, the turbulent region above the roofs is higher and the wind speeds in the streets are observed to be much lower than in the corresponding reference case.

3.2 Flow properties within the test street canyon

We find that for all the geometries chosen in this study, a single vortex appears in the street canyon. These kinds of flows would traditionally be modelled as a "regular" street canyon. The above comparison of flow patterns shows that for pitched roofs, which have rise-to-run ratios up to 6:12, some differences in flow properties do occur. These have implications for pollution accumulation in the street, which is determined not only by flow patterns but also by the flow properties.

This section focuses on analysing three flow properties that indicate the strength of the mean flow and its turbulence, namely horizontal velocity (U), vertical velocity (W) and turbulent kinetic energy (k). Figure 3.2, Figure 3.3 and Figure 3.4 below show the vertical profiles of these three flow properties in the test street for the cases with AR=1.0. All the results are normalized by the free-stream velocity U_0=7m/s, which is the velocity in the approach flow before the buildings, at roof height – roof height being defined as the height of the roof eaves, which is 12m throughout the study. The reference case is presented in black circles. In all cases there is a systematic change in the flow properties as the pitch rise, R, increases. This is noted on the graphs with arrows noting the direction of increasing R.

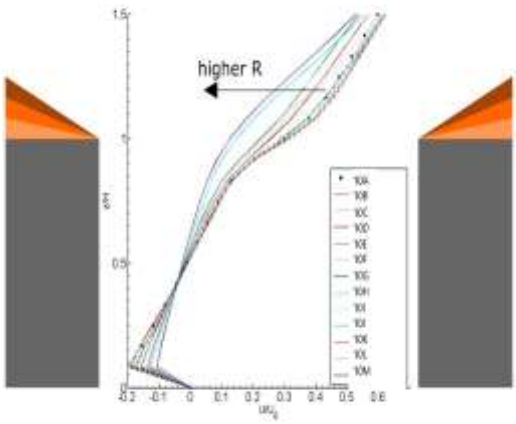

Figure 3.2: Normalized horizontal velocity U/U_0 vertical profile on the mid vertical line in the third street canyon.

It can be seen in Figure 3.2 that as the pitch rise R increases, the horizontal velocity above the center of the vortex and above the rooftop level at the top of the canyon decreases. Furthermore, as the pitch rise R increases, the vortex centre position, which is indicated by U=0 in Figure 3.2, moves upwards It is apparent in Figure 3.2 that for six cases the horizontal velocity above the roof level is comparable to the reference case. However, there are six cases (cases 10D, 10G, 10J and 10M, noted on the graph by four solid lines, and cases 10I and 10L noted by a cyan dotted line and a purple dotted line respectively) that have noticeably smaller horizontal velocity above roof level than the reference case. These are cases with roofs which have relatively large rise-to-run ratio, indicating that only pitched roofs with sharp slope lead to weaker horizontal advection at roof height compared with flat roofs. This might explain the previous findings by Rafailidis (1997) as discussed in the introduction.

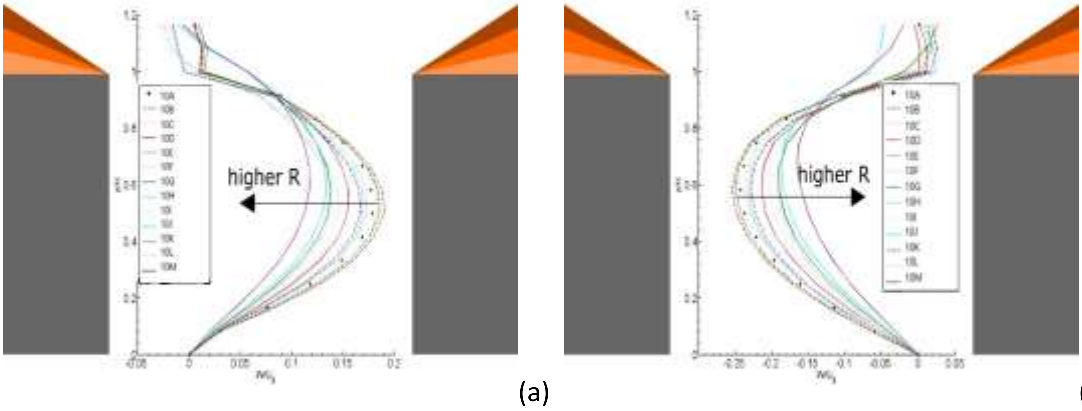

(a) (b)

Figure 3.3: Normalized vertical velocity W/U_0 in the third street canyon on two vertical profiles: (a) leeward side profile, taken 0.7m away from the leeward building and (b) windward side profile, taken 0.7m away from the windward building.

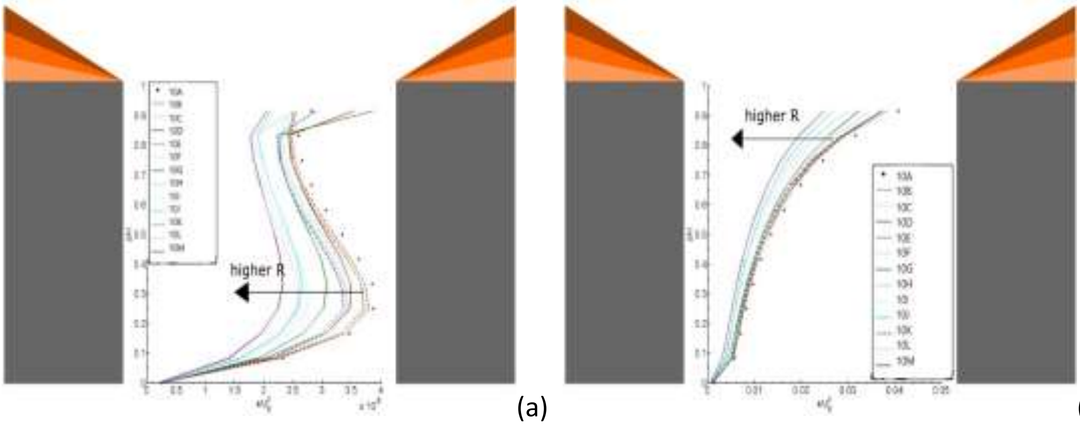

(a) (b)

Figure 3.4: Normalized turbulent kinetic energy k/U_0^2 in the third street canyon on two vertical profiles: (a) leeward side profile, taken 0.7m away from the leeward building and (b) windward side profile, taken 0.7m away from the windward building.

As can be noted from Figure 3.2 and Figure 3.3, higher pitch rise systematically leads to markedly lower vertical velocities throughout the street. We see that the previously mentioned six cases also have much smaller horizontal velocities and vertical velocities inside the street than the reference case and the other cases. This suggests that the strength of the mean flow in the street might be highly dependent on the flow intensity above the roof. There is no systematic difference between these six cases and the others where the vertical velocity above rooftop is concerned, although 10J and 10M generally have the highest vertical velocities above rooftop amongst the cases. Overall, the vertical velocities above rooftop height deviate only slightly from zero, indicating that vertical advection is not a strong mechanism for air exchange at these heights.

This correlation does not hold true for the turbulence in the street, as shown in Figure 3.4. For example, in Figure 3.2 and Figure 3.3, Case 10D (solid red line) shows very different velocity profiles from the reference case; however, in Figure 3.4 we see that these two cases have very similar TKE profiles on the windward vertical profile (and very different profiles on the leeward side). There is no systematic relationship between the other 5 cases in this group, where TKE is concerned. One possible explanation is that the turbulence inside the street canyon is mainly affected by local production rather than by the flow conditions outside the street. Once again however, the higher pitch rise systematically leads to noticeably lower turbulence inside the street.

We observe in figure 3.3a for the vertical profile on the leeward side that at the height of 0.45 to 0.5, the maximum value for the normalized vertical velocity is achieved for almost all the curves. This corresponds to the mid-point between the top and bottom boundaries of the vortex. It seems that this feature holds for all case studies regardless of roof shape.

The significance of roof morphology is apparent when the rise-to-run ratio is relatively large. We observe that all cases with a pitched roof on the leeward building (cases H, I, J, K, L, M in cyan and purple) have noticeably lower velocities and turbulence than the equivalent cases with the same rise-to-run ratio and the same roof structure on the windward building (cases B, C, D, E, F, G in red and green). On the other hand, the presence of a pitched roof on the windward building leads to slightly lower velocities and turbulence than the presence of a flat roof on the windward building. These results are consistent with the findings discussed in the introduction, by Huang et al (2009), and suggest that the roof shape on the leeward building has a major impact on the flow and turbulence in the street canyon, and the roof shape on the windward building has a minor impact.

3.3 Ventilation efficiency for the test street

The analyses of flow properties in the last section provide useful information about how different roof structures affect the strength of the mean flow and its turbulence in the test street canyon. In this section, two bulk parameters, the Exchange Velocity (U_E) and the Advection Velocity (U_A), are proposed to determine the ventilation efficiency of the test street canyon.

The exchange velocity (U_E) was proposed by eg Hamlyn and Britter (2005) as a parameter that characterises and quantifies pollutant removal rates from street canyons, that takes into account the airflow rate going into and out of a defined volume across a boundary plane. It has been used to assess city breathability in Buccolieri et al. (2010), and for heterogeneous urban geometries by Panagiotou et al. (2013). There have been since various definitions in the literature for exchange velocities, accounting for the airflow rate alone or for both airflow and the pollutant distribution. On a larger scale, mean Exchange velocities have been determined experimentally by Neophytou et al., 2014 to characterise and quanity the exchange processes and breathability of urban street canyon geometries with different packing densities. These and other studies have been recently reviewed in depth by Kubilay et al (2017).

The exchange velocity in our study follows the definition by Hamlyn and Britter (2005) and indicates the air exchange efficiency across the street opening, accounting as well for the turbulent flux terms. It is defined as the total momentum flux integrated across an exchange plane, divided by the difference between the mass flux above and below that plane. In two dimensional form this is given by:

$$U_E = \frac{\int_{L_c}(\rho\overline{uw}+\rho\overline{u'w'})\ dS}{\rho L_c(U_{ref}-U_c)} \quad (1)$$

where *u*, and *w* are the mean velocity components in the free-stream direction (m/s), span-wise direction and the direction normal to the ground respectively; *u'*, and *w'* are the fluctuating velocity components, ρ is the density of air (kg/m^3), L_c is the width of the exchange plane (m^2). Here, for geometric consistency across the different case studies, this is taken across the street opening, which is the horizontal plane at rooftop level, at the height of the eaves. This formulation results in an exchange velocity that is similar for streets with different Aspect ratios and thus is less dependent on geometry; thus this formulation illustrates the differences amongst the case studies only based on roof shape and street morphology. U_{ref} is the reference velocity, taken in this case to be U_0. U_c is the characteristic velocity, and here we define this as the average velocity magnitude below the exchange plane. The normalised exchange velocity for each case is shown in Figure 3.5a below.

The advection velocity (U_A) represents the average rotating speed of the vortex flow inside the street canyon and indicates the strength of the advection between the leeward and windward parts. We follow the definition proposed by Takano and Moonen (2013) which is defined as average absolute horizontal velocity along the mid vertical line from the bottom to the building height:

$$U_A = \frac{\int_{L_m}|u|\ \ dl}{L_m} \quad (2),$$

where L_m is the length of the mid vertical line. In the case of airflow with one vortex, the horizontal flow rate through the central vertical profile is a good approximation for the total volume of air which is rotating in the main vortex per unit of time. This formulation allows for consistency across the various case studies as they vary in terms of the height of the centre of the vortex and the total height of the vortex, but what they all have in common is a symmetry about the central vertical line. This allows the comparison across the cases to relate more to the differences in roof structure and street morphology.

The normalised advection velocity for each case is shown in Figure 3.5**Error! Reference source not found.**b below. The comparison between the exchange velocity and advection velocity, is presented in Figure 3.5c below for all cases.

As can be seen from Figure 3.5**Error! Reference source not found.**a, the exchange velocity is almost independent of the aspect ratio, which is consistent with the manner in which it has been defined, but it does relate to both roof slope and roof morphology. The variation of the exchange velocity due to different roof slopes and roof morphologies is quite significant. Case M always has the lowest exchange velocity; the reference case A is always the highest of all cases and is around four times as high as the Case M. We see here that the overall exchange velocity is unrelated to the average vertical velocities above rooftop height; in Figure 3.3 Cases J and M had been identified as having higher vertical velocities than most cases yet they result in the lowest exchange velocity.

Examining the results in detail, the relationship of exchange velocity to roof slope becomes significant when the leeward building has a pitched roof (cyan and purple bars in Figure 3.5a). For these roof morphologies, larger rise-to-run ratio means significantly lower exchange velocity. It can also be seen in Figure 3.5c, that the cases with large rise-to-run ratio show high sensitivity to roof morphology. For these cases, the presence of pitched roof on the leeward building leads to significantly lower exchange velocities.

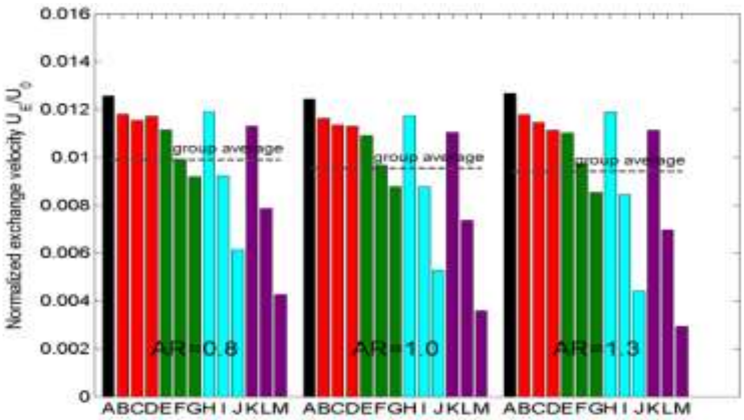

(a)

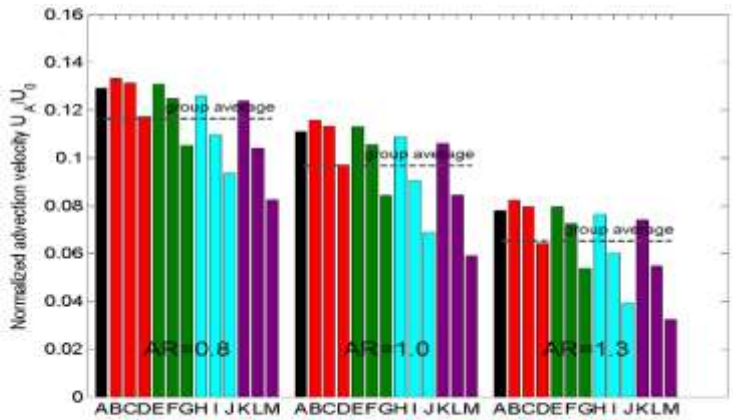

(b)

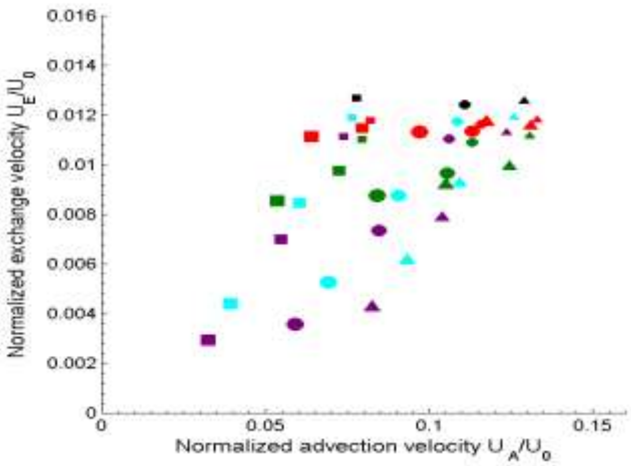

(c)

Figure 3.5 (a): Normalized exchange velocity U_E/U_0 for the third street for all the cases A to M (b): Normalized advection velocity U_A/U_0 for the third street for all the cases A to M. (c): Normalized exchange velocity U_E/U_0 and normalized advection velocity U_A/U_0 for the test street for all cases A to M. Square: AR=1.3, circle: AR=1.0, and triangle: AR=0.8; the symbol size is scaled as the rise-to-run ratio. The colour scheme in the three graphs is as outlined in section 2.4: Black (reference case): flat roofs on all the buildings, Red: flat roofs on the Leeward Building (LB) and on the Windward Building (WB), Green: flat roof on the LB and pitched roof on the WB, Cyan: pitched roof on LB and flat roof on the WB, Purple: pitched roof both on the LB and on the WB

In Figure 3.5b, we see that roof slope and roof morphology have a similar effect on the advection velocity as was seen in Figure 3.5a for the exchange velocities. However, the aspect ratio affects the advection velocity more significantly. In general, the cases with a larger aspect ratio have lower advection velocity, indicating these cases have poorer advection between the leeward and windward parts even when they have similar exchange efficiency at the street opening. This finding is consistent with the difference in vortex size and speed for street canyons with different aspect ratios and would have implications for pollution dispersion within the street.

Figure 3.5**Error! Reference source not found.**c compares the exchange velocity with the advection velocity, demonstrating that the air exchange between the street canyon and the atmosphere is somewhat positively related to the strength of the advection due to the vortex flow. The red cases (B, C, and D), all have pitched roofs in the background but flat roofs on both sides of the test street. The results for these cases are closest to those for the reference case, noted by black symbols. For all other roof morphologies, some interesting observations can be made.

The cases with a small rise-to-run ratio, noted on the graph using smaller symbols, are clustered at the top of Figure 3.5c; these comprise around half of the cases and they exhibit high exchange velocities, and advection velocities which are comparable to the velocities for the reference cases. Thus, cases where the roofs are close to flat have the best ventilation. The other scattered points are the cases with relatively large rise-to-run ratio and pitched roofs on the leeward building and/or the windward building. Both exchange velocity and advection velocity are lowest when the leeward building has a pitched roof with sharp slope, as can be seen for the six cyan and purple points in the bottom part of Figure 3.5**Error! Reference source not found.**c; here we observe a significant reduction in ventilation.

In all cases, the presence of pitched roofs leads to less efficient ventilation than the reference case. In addition, the presence of pitched roofs causes higher average concentrations for the whole street in most cases. This trend is more significant for the third (test) street canyon than for the fourth, downstream street canyon.

3.4 Pollutant distribution

The pollutant distribution for a typical case, Case 10M, is compared with the reference Case 10A in Figure 3.6 below. The concentration is presented in a normalized form as:

$$c^* = \frac{cU_0H}{Q/L_q} \quad (3)$$

where c is the pollutant concentration (kg/m^3), Q is the emission rate (kg/s), L_q is the length of the source (m), U_0 is the free-stream velocity (m/s), and H is the building height (m).

Figure 3.6 shows airflow patterns for the reference case 10A and for Case 10M. The sources are defined as 0.3m wide (equivalent to 0.025H, where H is the height of the building up to the roof eaves) and are placed 1m away from the leeward building and 1m away from the windward building at height 0.025H. As expected, for both cases concentration is higher on the leeward side than on the windward side due to the vortex flow pattern. The concentration is higher in the fourth street canyon than in the third street canyon, as some of the pollutants removed from the third street are entrained into the fourth street in addition to the local source in the fourth street. The differences between Case 10A and Case 10M are not large at first examination, but a more detailed analysis reveals systematic variations that would have significant implications for pedestrians and residents in a street under prolonged exposure to local sources of pollution.

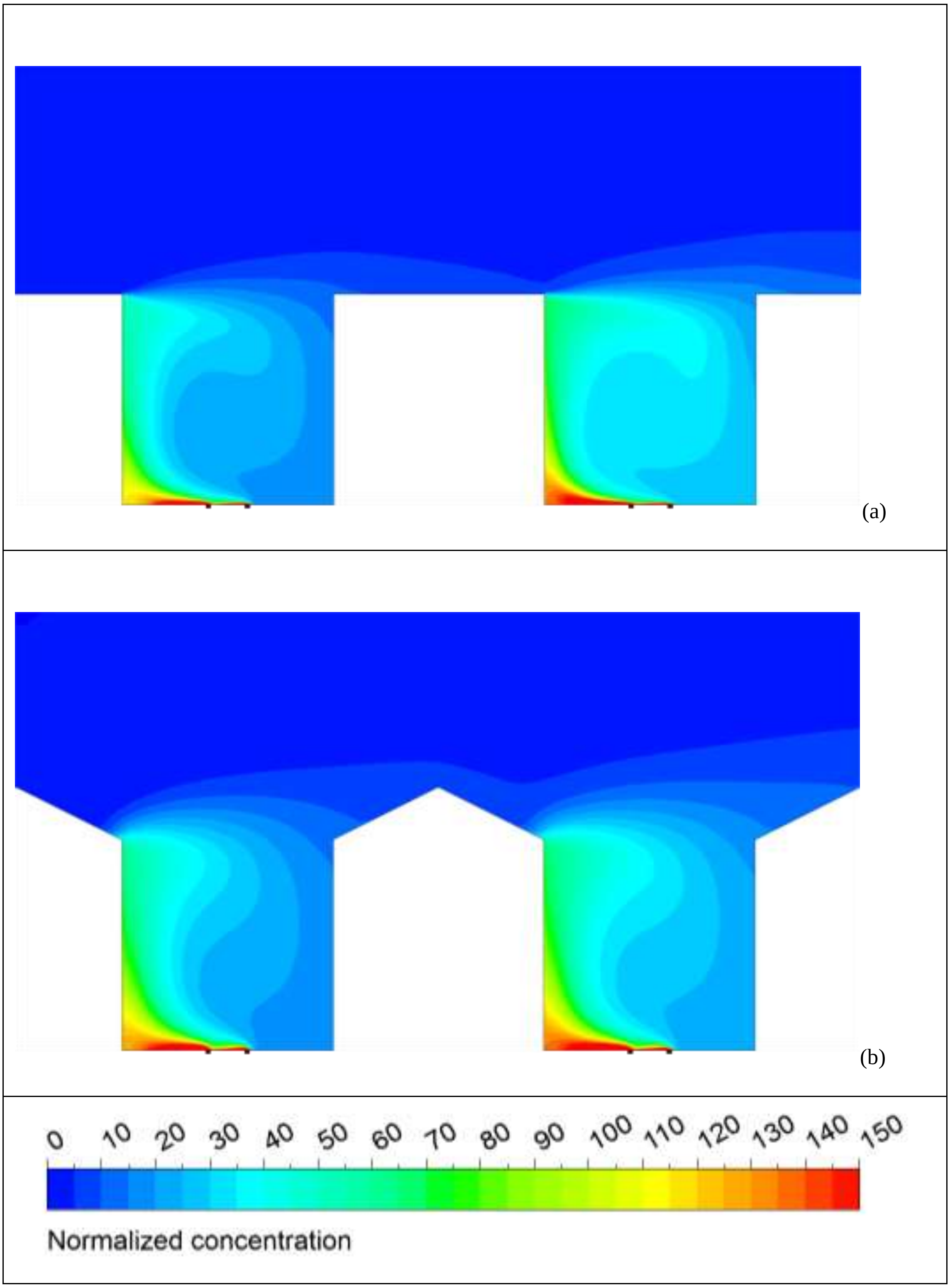

Figure 3.6: Normalized concentration contour around the third and the fourth street canyons: (a) Case 10A (reference) and (b) Case 10M. The sources are noted as small black squares in the street canyons. The sources are defined as 0.3m wide (equivalent to 0.025H, where H is the height of the building up to the roof eaves) and are placed 1m away from the leeward building and 1m away from the windward building at height 0.025H

3.5 Average concentrations within the street canyons

The following section presents a detailed comparison of pollutant concentrations between cases. The bar charts in Figure 3.7 display the average concentration of the whole street. Figure 3.8 shows in two cases the ratio of the concentration in the third street canyon to the reference case. The contour plots in Figure 3.8 reveal concentration differences across the street at a fine resolution. The 'heat-maps' in Figure 3.9 show the concentration difference between all cases in different parts of the street canyon.

It is observed from Figure 3.6, Figure 3.7a and Figure 3.7b that the average concentration for the fourth street is around 20% higher than for the third street canyon, for all cases, because some of the pollutants removed from the third street are re-entrained into the fourth street. For both streets, the aspect ratio is the primary factor determining concentration. For all roof configurations, the larger the aspect ratio H/W of building height to street width, the higher the average concentration within the street. This concentration can be twice as high for some of the comparable cases, such as 13M versus 08M.

It is seen from Figure 3.7a that in 34 out of 36 cases, the average concentration in the third street is higher than the corresponding reference case; similarly, for the fourth street, 27 of 36 cases have higher average concentration than the corresponding reference case. The increments for both streets are typically within 10%. Therefore, clearly pitched roofs are generally adverse for pollutant removal in street canyons. In particular, there are a few cases such as Cases 13J and 13M, which have increments of more than 25%.

It is further observed from Figure 3.7a and Figure 3.7b that for a specified rise-to-run ratio, the placement of a pitched roof on the leeward building (cyan and purple bars in the figures) leads to higher average concentrations in both the third and the fourth street canyons, than when the pitched roof is on the windward building (green bars in both figures and red bars in Figure 3.7b). This trend becomes more obvious for a larger aspect ratio.

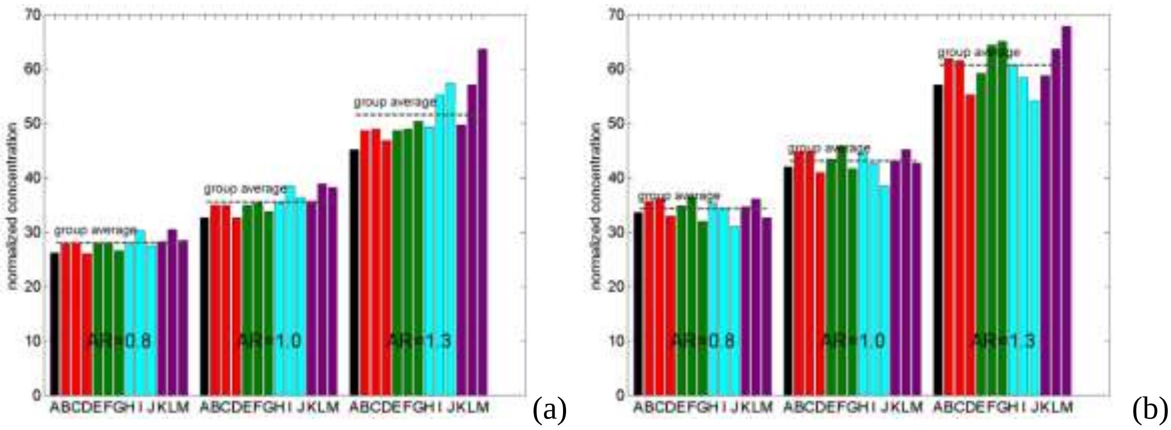

Figure 3.7: Normalized average concentration for all the cases A to M for (a) the third street canyon and (b) the fourth street canyon, with aspect ratio 0.8, 1.0 and 1.3. The colour scheme is as outlined in section 2.4: Black (reference case): flat roofs on all the buildings, Red: flat roofs on the Leeward Building (LB) and on the Windward Building (WB), Green: flat roof on the LB and pitched roof on the WB, Cyan: pitched roof on LB and flat roof on the WB, Purple: pitched roof both on the LB and on the WB

It is surprising to find from Figure 3.7 (a) that for the third street, 9 out of the 12 cases with a rise-to-run ratio of 4:12 (i.e., Cases 08C, 08F, 08I, 08J, 10C, 10F, 10I, 10L, 13C) have even higher average concentration throughout the street than the corresponding cases with a rise-to-run ratio of 6:12 and the same roof morphology. This does not seem consistent with the previous finding that for the same roof morphology, the larger the rise-to-run ratio is, the lower the flow properties such as exchange velocity and advection velocity – which would be expected to lead to higher concentrations in those cases.

This issue can be explained by examining the ratio of the concentration of those cases to the concentration of the reference case. The contours for four typical cases, Cases 10L, 10M, 13L and 13M are shown in Figure 3.8 below. For Case 10L (see Figure 3.8a), the pitched roofs with rise-to-run ratio of 4:12 increase concentration by around 20% at most positions. In contrast, for Case 10M (see Figure 3.8b), the pitched roofs with rise-to-run ratio of 6:12 increase the concentration in the leeward part and above the emission sources significantly, over 50% higher in some parts of the street, but reduce the concentration in the windward part only slightly (less than 5%). Thus, it is seen that Case 10L has higher average concentration for the entire cross section than Case 10M, but case 10M has pollution hotspots with much higher localised concentrations. This effect is more pronounced for Cases 13M and 13L. The higher concentrations are the source of concern for air quality and its links to public health.

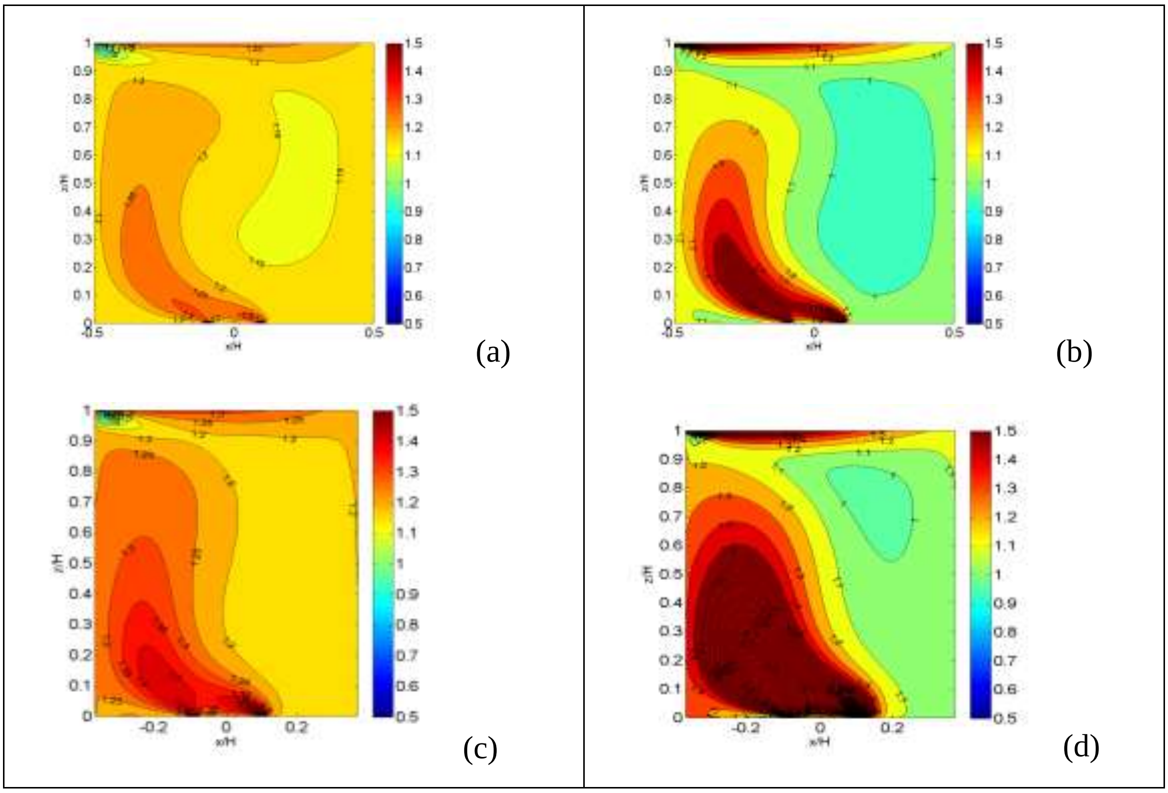

Figure 3.8: The ratio of concentration (Cr) in the third street canyon to that of the reference case, (a) Case 10L and (b) Case 10M. (c) Case 13L and (d) Case 13M.

Table 3-1 below summarises the average normalised concentrations for the reference cases, averaged over the entire third and fourth street canyons. It can be seen that the fourth street canyon has on average 26%-28% higher pollution concentrations than the third one. This difference persists for all three cases at different aspect ratios.

Aspect Ratio	Third street	Fourth street	Difference %
0.8 – wide street	26.2	33.6	28
1.0	32.7	42.0	28
1.3 – narrow street	45.3	57.1	26

Table 3-1 Average normalized concentrations in the reference cases, comparing the third and fourth streets

To better understand the detailed pollution distribution and detect concentration hot spots for all cases, we present "heat maps" of Cr in the street canyons for all case studies and all parameters below. The third and fourth streets are equally divided into eight rectangular sections, each of which is 3m tall and half a street wide. Thus, assuming buildings that height are normally roughly four floors high, each of these sections corresponds to an adjacent outdoor space for each floor of the leeward building or the windward building. We calculate Cr separately for each section and for each case. The cases for aspect ratio 0.8 are shown at the top, under which appear respectively the cases for AR=1.0 and AR=1.3. The resulting increments are up to ±28%. The results for the third and the fourth street canyons are displayed as coloured blocks in Figure 3.9 below.

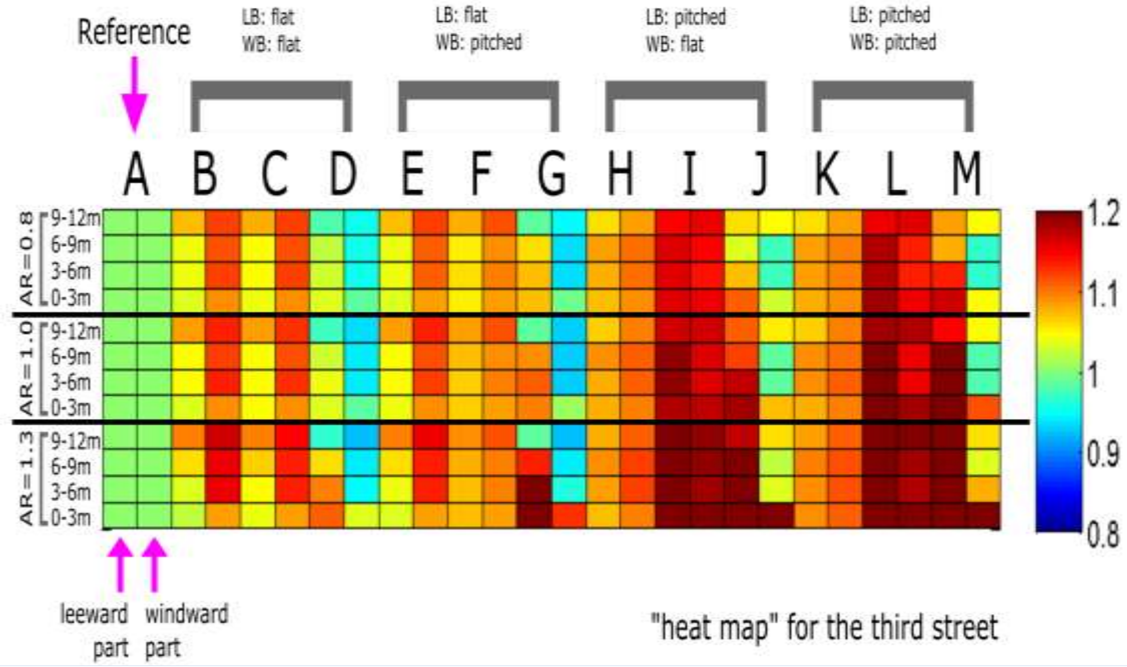

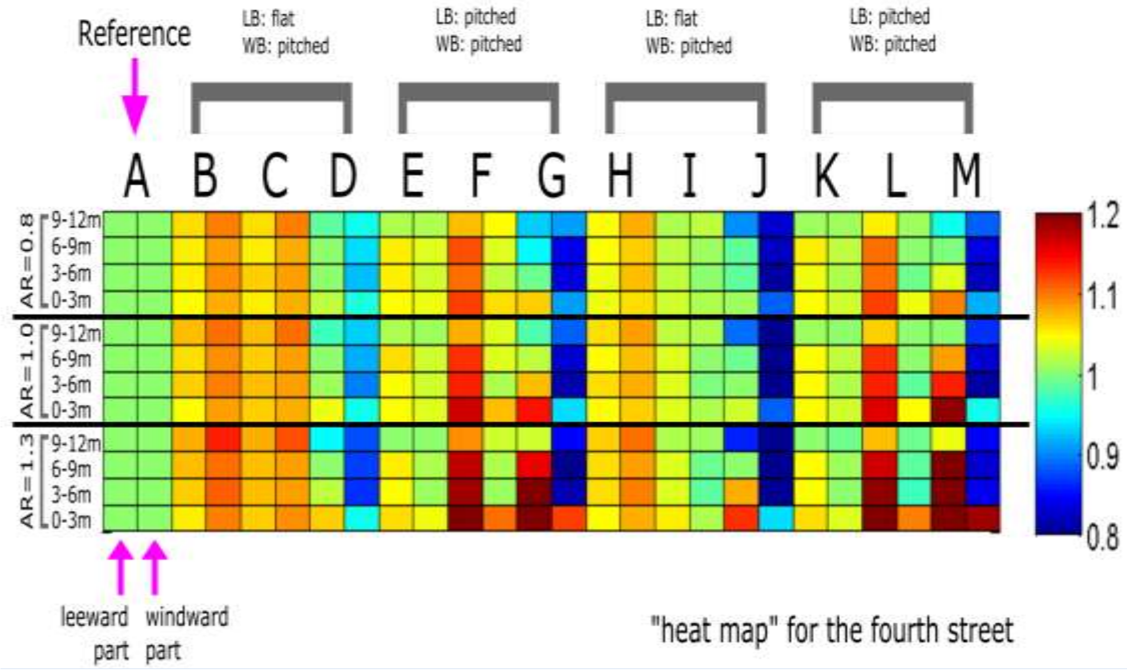

Figure 3.9: The “heat-maps” of Cr for the third street (top) and the fourth street (bottom). WB denotes Windward Buildings and LB denotes Leeward Buildings

As can be seen in the top heat map in Figure 3.9, the presence of pitched roofs causes higher concentration than the reference case in most sections of the third street for all cases. When pitch rise is low or medium, the concentration increases in all sections of the street. The increments are up to 15% and are higher in all cases in the windward sections of the street. The exception is the cases with medium-rise pitched roof on the leeward building. (i.e., Cases I and L for all aspect ratios). In these cases, the increments are much higher, leading to increases of 15–25%, on both the windward and the leeward sections. When pitch rise is high (Cases G, J and M for all aspect ratios), concentration increases by 15-25% in the leeward part and near the ground floor of the windward building, but is conversely up to 10% lower than the reference near the first and the second floors of the windward building.

It is interesting to examine the fourth street as well. This street has its own pollution source and also appears to have additional pollution entrained into it from the third street. The average concentrations in this street are consistently higher than for the third street, as seen in Figure 3.7. In all cases this street has pitched roofs on the windward buildings. As can be seen in the bottom heat map in Figure 3.9, the presence of pitched roofs causes higher concentrations in some sections of the fourth street, as it did for the third street. However, this is less systematic than for the third street, and the increments are much smaller in all cases. It can be seen that the high-rise pitched roofs (Cases D, G, J and M for all aspect ratios) lead to significant reduction in concentrations in the windward sections of *both* streets – both the third street and the fourth street, but the increment reductions are far greater on the fourth street. This finding suggests that high-rise pitched roofs might benefit air quality in a downstream street canyon. As a consequence, most of the cases with high pitch rise – 18 out of 24 - have reduced average concentration, which is seen in the bar charts in Figure 3.7.

Furthermore, it is interesting to compare cases E,F,G for the third street, with cases H,I,J in the fourth street. In these cases the streets in question are morphologically the same, respectively (see Figure 2.3) but as the approaching flow is different, the detailed concentrations resulting within the streets are different. It is true that both cases where there is a flat roof on the leeward building (LB) and low rise pitched roof on the WB: case E (third street) and case H (fourth street), present higher concentrations on the windward side. On the other hand, the cases with flat roof on the LB and high rise pitched roof on the WB: cases G (third street) and J (fourth street) both have notably reduced concentrations on the windward side, though the increments are very different. But Case F (third street) and I (fourth street), though both have flat roof on the LB and mid-rise pitched roof on WB, are not comparable in terms of the resulting concentrations.

4 Discussion

It is worth considering whether the RANS approach and the k-epsilon model are justified for the case of pitched roofs. The limitations of these models have been discussed in the literature and are summarised effectively by Kubilay et al (2017). We found that these are appropriate for the case studies in the parameter space studied, as the rise-to-run ratios are not very sharp and we do not find a very strong flow separation at the roof ridge; unsteady and complex flow is less prevalent and it is still reasonable to assume isotropic turbulence in these cases. For higher pitch roofs these assumptions would be more precarious and it would be more appropriate to use a transient model such as Large Eddy Simulation. An LES simulation would also lead to better resolution of the full flow details including for example the thickness of the shear layer for every geometry. However, these simulations are still time consuming and expensive to run and would be prohibitive for a study attempting to investigate a larger parameter space as we have attempted here. It is noteworthy that Karra et al (2017) modelled in the laboratory a heterogeneous street canyon with variation along the length of the street and strong step down and step-up features leading to flow separation. The physical model showed that on an instantaneous time scale, velocity and concentration fields demonstrate the dissolving and reconstructing at short intervals, but that on average, the underlying vortex structure is persistent.

In our study, the streets were modelled in 2D as the streets are homogeneous throughout. Karra et al (2017) demonstrate for a heterogeneous street that although there is a measurable three dimensional flow over the street as a whole, every section of the street has within it a strong underlying two dimensional structure and a basic vortex as expected. This gives us confidence that despite the introduction of a sloping roof, we can assume a fundamental underlying flow that is homogeneous along the length of the street, anda two-dimensional CFD model is representative.

In all cases it is clear in our results that pitched roofs within the range studied, of 2:12 – 6:12, always reduce ventilation, lower velocities and turbulence within the street and lead to higher pollution concentrations. There are two specific geometrical features that lead to even worse ventilation in this range of pitched roofs:

1. High pitch rise: for any given urban roof morphology, the higher the pitch rise the larger the observed reduction in velocities and turbulence and thus, the lower the ventilation efficiency. This is consistent with the thicker shear layer in the high pitch rise cases and the overall reduction in flow separation compared with the flat roof case. Kubilay et al (2017) discuss the importance of the shear layer generated at the rooftop level in determining the air flow and pollutant dispersion within and above urban street canyons. This shear layer is closely attributed to roughness arising at the roof surfaces, the full resolution of which is beyond the scope of this study.
2. Placing pitched roofs on the leeward side of the street: the very worst cases for pollution are when the pitched roofs are on the leeward side, especially when the pitch rise is the medium pitch of 4:12.

According to our results, it can be considered that turbulent exchange at the rooftop level plays a significant role in air exchange, and the increase of pitch-to-rise ratio especially has a negative impact on turbulent exchange and thus on overall air exchange. Table 4-1 below presents the mean flux and turbulence flux for three typical cases: 10A, 10J and 10M, indicating fluxes upwards and out of the street canyon. Although the pitched roofs with rise-to-run ratio of 6:12 in Cases 10J and 10M lead to a higher mean flux compared with the reference case, they have a much stronger impact on the turbulence flux. The turbulence flux in these two cases is reduced by more than 65% compared with the reference case, leading to a reduction in *total* flux of more than 50%.

Case	Mean flux uw	Turbulence flux $u'w'$
10A	-0.39	-7.37
10J	-0.83	-2.61
10M	-0.46	-1.91

Table 4-1 The mean flux and turbulence flux for three typical cases: The reference case 10A, and cases 10J and 10M

These findings are consistent with Kubilay et al. (2017), yet it is important to note that as they discuss, it has been found in several studies that the RANS k-ε model is limited in its ability to fully predict the turbulent flow in the shear layer region, with under-prediction of turbulent diffusion of pollutants in the shear layer and under-prediction of turbulent kinetic energy in the wake of the buildings.

5 Conclusion

This paper studied the impact of pitched roofs on airflow and pollutant dispersion in street canyons via a parametric approach. Three parameters were defined, namely the aspect ratio of building height to street width, the pitch rise and the roof morphology. The impact on airflow was analysed on the basis of flow patterns and flow property profiles within the street, as well as advection velocity and exchange velocity as two indicators of ventilation efficiency for the street as a whole.

We find that the detailed impact of pitched roofs varies widely; it depends on roof morphologies, pitch rise and the combination of these factors. In all cases it is clear that pitched roofs within the range studied, of 2:12 – 6:12, always reduce ventilation, lower velocities and turbulence within the street and lead to higher pollution concentrations. For any given urban roof morphology, the higher the pitch rise, the lower the velocities and turbulence and thus, the ventilation efficiency. The very worst cases for pollution are when the pitched roofs are on the leeward side, especially when the pitch rise is the medium pitch of 4:12.

The impact on pollutant dispersion was presented with respect to the average concentration for the whole street, the average concentration for different sections of the street and the deviation of concentration from the reference case throughout the street. This type of detailed parametric analysis and presentation via "heat maps" allows a useful exploration of the parameter space and an understanding of the sensitivity to various parameters and their combination.

It would be desirable to have a set of experiments with at least a few test runs for the various roof slopes to cover the parameter space. Such experiments are costly and time-consuming to run. The purpose of a parametric CFD study is to go beyond the available experimental datasets and explore the parameter space further. It is hoped that this study provides justification for attempting the experiments and can inform the selection of interesting parameters for an experimental or field study.

It is clear from examining the fourth street that rules of thumb regarding the ventilation and pollution distribution in various street morphologies need to be treated with caution. We find that pollution that is ventilated out of one street canyon becomes entrained into an adjacent downstream street canyon and raises local concentrations there further. Furthermore, the resulting pollution concentrations in both examined street canyons are different and are highly sensitive to these local parameters: both sources in the upstream flow as well as to the local morphology of the street in question. Roof morphology, the number of preceding streets in the upstream flow, the height of the roofs and whether they are on the leeward or windward side of the street all have a substantial effect on the pollution concentrations within the street and on the way these are distributed across the street in relation to width and height. Furthermore, in a typical street canyon there are many additional local factors that would affect airflow and concentrations. It appears that for a sophisticated and highly accurate analysis of any given street there is no substitute for a bespoke 3D CFD simulation, one which models transient flow and models the turbulent diffusion carefully.

There is a case for bespoke models of urban environments: the surrounding environment and the local parameters within the street must always be carefully modelled when attempting to predict build-up of pollution and heat within any given street canyon. This is not feasible for most urban locations, and for many standard urban settings the general rules of thumb in street canyon studies provide good guidance. However, there may be significant implications to health and wellbeing when local concentrations of heat and pollution in micro-environments are persistently high. High localised pollution concentrations due to poor urban design might also cause continuous damage to buildings of significant historical and cultural importance. Thus, for urban areas of high value or with high human traffic, full scale models, validated by corresponding experiments and field data, are well worth consideration.

This research did not receive any specific grant from funding agencies in the public, commercial, or not-for-profit sectors.

REFERENCES

ANSYS INC. 2009. ANSYS FLUENT 12.0 Theory Guide. U.S.A.: ANSYS, Inc.

BUCCOLIERI, R., SANDBERG, M. & DI SABATINO, S. 2010. City breathability and its link to pollutant concentration distribution within urban-like geometries. *Atmospheric Environment,* 44**,** 1894-1903.

FRANKE, J., HELLSTEN, A., SCHL NZEN, H. & CARISSIMO, B. 2007. Best Practice Guideline for the CFD Simulation of Flows in the Urban Environment: COST Action 732 Quality Assurance and Improvement of Microscale Meteorological Models.

GROMKE, C. & BLOCKEN, B. 2015. Influence of avenue-trees on air quality at the urban neighborhood scale. Part I: Quality assurance studies and turbulent Schmidt number analysis for RANS CFD simulations. *Environmental Pollution,* 196**,** 214-223.

GU, Z.-L., ZHANG, Y.-W., CHENG, Y. & LEE, S.-C. 2011. Effect of uneven building layout on air flow and pollutant dispersion in non-uniform street canyons. *Building and Environment,* 46**,** 2657-2665.

GUILLAS, S., GLOVER, N. & MALKI-EPSHTEIN, L. 2014. Bayesian calibration of the constants of the – turbulence model for a CFD model of street canyon flow. *Computer Methods in Applied Mechanics and Engineering,* 279**,** 536-553.

HAMLYN, D. & BRITTER, R. 2005. A numerical study of the flow field and exchange processes within a canopy of urban-type roughness. *Atmospheric Environment,* 39**,** 3243-3254.

HUANG, Y., HU, X. & ZENG, N. 2009. Impact of wedge-shaped roofs on airflow and pollutant dispersion inside urban street canyons. *Building and Environment,* 44**,** 2335-2347.

KARRA, S., MALKI-EPSHTEIN, L., NEOPHYTOU, M.K.-A., 2017. Air flow and pollution in a real, heterogeneousurban street canyon: A field and laboratory study. *Atmospheric Environment,* 165, 370-384.

KASTNER-KLEIN, P. 1999. Description of wind tunnel studies on flow field and dispersion characteristics in street canyons at the University of Karlsruhe.

KASTNER-KLEIN, P., BERKOWICZ, R. & BRITTER, R. 2004. The influence of street architecture on flow and dispersion in street canyons. *Meteorology and Atmospheric Physics,* 87**,** 121-131.

KASTNER-KLEIN, P. & PLATE, E. J. 1999. Wind-tunnel study of concentration fields in street canyons. *Atmospheric Environment,* 33**,** 3973-3979.

KOUTSOURAKIS, N., BARTZIS, J. G. & MARKATOS, N. C. 2012. Evaluation of Reynolds stress, k-ε and RNG k-ε turbulence models in street canyon flows using various experimental datasets. *Environmental Fluid Mechanics,* 12**,** 379-403.

KUBILAY, A., NEOPHYTOU, M.K.-A., MATSENTIDES, S., LOIZOU, M., CARMELIET J.,2017, The pollutant removal capacity of urban street canyons as quantified by the pollutant exchange velocity, *Urban Climate*, 21, 136-153.

LEITL, B. M. & MERONEY, R. N. 1997. Car exhaust dispersion in a street canyon. Numerical critique of a wind tunnel experiment. *Journal of Wind Engineering and Industrial Aerodynamics,* 67–68**,** 293-304.

LLAGUNO-MUNITXA, M., BOU-ZEID, E. & HULTMARK, M. 2017. The influence of building geometry on street canyon air flow: Validation of large eddy simulations against wind tunnel experiments. *Journal of Wind Engineering and Industrial Aerodynamics,* 165**,** 115-130.

LOUKA, P., BELCHER, S. E. & HARRISON, R. G. 1998. Modified street canyon flow. *Journal of Wind Engineering and Industrial Aerodynamics,* 74–76**,** 485-493.

MERONEY, R. N., PAVAGEAU, M., RAFAILIDIS, S. & SCHATZMANN, M. 1996. Study of line source characteristics for 2-D physical modelling of pollutant dispersion in street canyons. *Journal of Wind Engineering and Industrial Aerodynamics,* 62**,** 37-56.

NEOPHYTOU, M. K.-A., MARKIDES, C. N., AND FOKAIDES, P. A., 2014. An experimental study of the flow through and over two dimensional rectangular roughness elements: Deductions for urban boundary layer parameterizations and exchange processes. *Physics of Fluids* 26, 086603

OKE, T. R. 1988. Street design and urban canopy layer climate. *Energy and Buildings,* 11**,** 103-113.

PANAGIOTOU, I., NEOPHYTOU, M. K. A., HAMLYN, D. & BRITTER, R. E. 2013. City breathability as quantified by the exchange velocity and its spatial variation in real inhomogeneous urban geometries: An example from central London urban area. *Science of The Total Environment,* 442**,** 466-477.

RAFAILIDIS, S. 1997. Influence of Building Areal Density and Roof Shape on the Wind Characteristics Above a Town. *Boundary-Layer Meteorology,* 85**,** 255-271.

REID, R. N. 2000. Roofing & Cladding Systems: A Guide for Facility Managers, USA, The Fairmont Press, Inc.

SCHMID, K. F. 2014. Concise encyclopedia of construction terms and phrases. *"Slope" def. 1.* New York: Momentum.

SINI, J.-F., ANQUETIN, S. & MESTAYER, P. G. 1996. Pollutant dispersion and thermal effects in urban street canyons. *Atmospheric Environment,* 30**,** 2659-2677.

SOLAZZO, E., CAI, X. & VARDOULAKIS, S. 2009. Improved parameterisation for the numerical modelling of air pollution within an urban street canyon. *Environmental Modelling & Software,* 24**,** 381-388.

TAKANO, Y. & MOONEN, P. 2013. On the influence of roof shape on flow and dispersion in an urban street canyon. *Journal of Wind Engineering and Industrial Aerodynamics,* 123, Part A**,** 107-120.

THEODORIDIS, G. & MOUSSIOPOULOS, N. 2000. Influence of Building Density and Roof Shape on the Wind and Dispersion Characteristics in an Urban Area: A Numerical Study. *Environmental Monitoring and Assessment,* 65**,** 407-415.

TOMINAGA, Y., MOCHIDA, A., YOSHIE, R., KATAOKA, H., NOZU, T., YOSHIKAWA, M. & SHIRASAWA, T. 2008. AIJ guidelines for practical applications of CFD to pedestrian wind environment around buildings. *Journal of Wind Engineering and Industrial Aerodynamics,* 96**,** 1749-1761.

TOMINAGA, Y., STATHOPOULOS, T. 2013 CFD simulation of near-field pollutant dispersion in the urban environment: A review of current modeling techniques. *Atmospheric Environment,* 79, 716-730

UEHARA, K., MURAKAMI, S., OIKAWA, S. & WAKAMATSU, S. 2000. Wind tunnel experiments on how thermal stratification affects flow in and above urban street canyons. *Atmospheric Environment,* 34**,** 1553-1562.

WEN, H. 2017. The Effect of Urban Geometries and Roof Shapes on Airflow and Pollutant Dispersion: A CFD Investigation. Doctor of Philosophy, University College London. http://discovery.ucl.ac.uk/1547519/

WEN, H., KARRA, S. & MALKI-EPSHTEIN, L. 2013. Modelling of street canyon geometries in CFD – A comparison with experimental results. *13th Conference of International Building Performance Simulation Association.* Chambery, France.

XIE, X., HUANG, Z. & WANG, J.-S. 2005. Impact of building configuration on air quality in street canyon. *Atmospheric Environment,* 39**,** 4519-4530.

YASSIN, M. F. 2011. Impact of height and shape of building roof on air quality in urban street canyons. *Atmospheric Environment,* 45**,** 5220-5229.